Re-entrant phase behaviour of network fluids: A patchy particle model with temperature-dependent valence

J. Russo,[1,a)] J. M. Tavares,[2,3] P. I. C. Teixeira,[2,3] M. M. Telo da Gama,[3,4] and F. Sciortino[1]
[1]*Dipartimento di Fisica and CNR-ISC, Università di Roma La Sapienza, Piazzale A. Moro 2, I-00185 Rome, Italy*
[2]*Instituto Superior de Engenharia de Lisboa, Rua Conselheiro Emídio Navarro 1, P-1950-062 Lisbon, Portugal*
[3]*Centro de Física Teórica e Computacional, Avenida Professor Gama Pinto 2, P-1649-003 Lisbon, Portugal*
[4]*Departamento de Física, Faculdade de Ciências da Universidade de Lisboa, P-1749-016 Lisbon, Portugal*

(Received 26 April 2011; accepted 10 June 2011; published online 15 July 2011)

We study a model consisting of particles with dissimilar bonding sites ("patches"), which exhibits self-assembly into chains connected by Y-junctions, and investigate its phase behaviour by both simulations and theory. We show that, as the energy cost ϵ_j of forming Y-junctions increases, the extent of the liquid-vapour coexistence region at lower temperatures and densities is reduced. The phase diagram thus acquires a characteristic "pinched" shape in which the liquid branch density decreases as the temperature is lowered. To our knowledge, this is the first model in which the predicted topological phase transition between a fluid composed of short chains and a fluid rich in Y-junctions is actually observed. Above a certain threshold for ϵ_j, condensation ceases to exist because the entropy gain of forming Y-junctions can no longer offset their energy cost. We also show that the properties of these phase diagrams can be understood in terms of a temperature-dependent effective valence of the patchy particles. © *2011 American Institute of Physics*. [doi:10.1063/1.3605703]

I. INTRODUCTION

In recent years the study of anisotropic interactions in simple fluids has led to an extraordinary progress in our understanding of the competition between self-assembly and phase separation. It is well known that, for particles interacting via isotropic potentials that comprise an excluded-volume repulsion and a long-range attraction, condensation occurs when the energy drop associated with forming a high-density liquid overcomes the concomitant loss of entropy. On the other hand, anisotropic interactions promote the aggregation of particles into self-assembled structures, such as chains, rings, and more complex clusters (e.g., micelles and vesicles). This aggregation process can compete with the clustering that drives condensation, giving rise to new phase behaviours. We will mention here two important examples where the competition between condensation and aggregation plays a dominant role.

The first example is provided by Janus colloidal particles,[1] i.e., particles which attract each other via just one-half of their surface (one hemisphere). The phase diagram of the disordered phases has been recently revealed,[2] showing that, at odds with a standard liquid-vapour phase separation, the vapour phase is composed of micelles which have a lower energy than the coexisting liquid. The self-assembly into micelles increases the stability of the vapour phase at higher densities with decreasing temperatures, progressively suppressing the two-phase region. A recent statistical mechanical model[3] has indeed confirmed the generality of this type of phase behaviour for systems where monomers assemble into monodispersed clusters with no attractive interactions to other species.

A second example in which the competition between condensation and aggregation can change the nature of the phase transition is given by ferrofluids[4–8] or electrorheological fluids, in which particles have an embedded permanent magnetic or electric dipole. In this case, the anisotropy of the dipolar interaction promotes the formation of long polymer-like self-assembled chains of particles, in contrast to the isotropic compact clusters observed in simple fluids. This type of aggregation interferes with the usual liquid-vapour transition because chain formation tends to saturate the dipolar attractions, leading to an effective screening thereof. In particular, for dipolar hard or soft spheres (DHSs or DSSs), the simplest models for dipolar fluids, in which a hard or soft sphere is complemented with a permanent dipole at its centre, there is still controversy over whether a liquid-vapour critical point exists. Numerical simulations[9,10] suggest that if such a critical point exists, it must be located at very low temperatures and densities, where the dipoles aggregate into linear and branched structures, and where the anisotropy of the interactions plays a dominant role. See, e.g., Ref. 11, and references therein, for a recent review.

In order to study the interplay between self-assembly and condensation systematically, a recent line of research has concentrated on the phase properties of patchy particles.[12–14] Patchy particles are particles whose surface is patterned so that they attract each other via discrete sites ("sticky spots") located on their surface. Among the advantages of patchy particles are their simplicity and the fact that the degree of anisotropy in the interactions can be fine-tuned by changing the number, type, size, and strength of the patches. However, the most important feature that makes patchy particles ideally

a)Author to whom correspondence should be addressed. Electronic mail: john.russo.mcdougall@gmail.com.

suited for our investigation is the fact that both their thermodynamic and structural properties can be predicted with a high degree of precision using the thermodynamic first-order perturbation theory of Wertheim[15,16] and the Flory-Stockmayer theory of polymerization.[17,18] It is thus possible to study the criticality of patchy particles from a standard liquid-state theory approach, without resorting to phenomenological theories.

It has been shown[19,20] that the location of the liquid-vapour critical point of patchy particles, under the single-bond per patch condition, is controlled by the average number of patches per particle, also called *valence*: by decreasing the valence, the critical point is shifted to lower temperatures and densities, and disappears for average valences ≤ 2. The possibility to shift the coexistence line to arbitrarily low densities has opened up the possibility to obtain stable liquids at vanishingly small densities (the so-called "empty-liquids"[20,21]), and most notably provided a means to study the equilibrium route to gelation.[22–24]

In order to investigate the interplay of condensation and different types of self-assembly, models with patches of two different types (2 A sites and 1 B site) were recently introduced.[25,26] Different types of criticality were revealed by varying the relative strengths of the attractions between like or unlike patches. Of particular interest are the cases where the self-assembling structures are composed of long polymer-like chains connected by junctions, as the liquid-vapour phase separation can then be viewed as the condensation of these junctions. Two types of junctions are possible in models where AA bonds are responsible for the chaining: X-shaped junctions, due to BB bonds, and Y-shaped junctions, due to AB bonds. Furthermore, it has been shown that, whereas X-junctions always (never) yield a critical point if their formation is energetically favourable (unfavourable), Y-junction fluids will exhibit a critical point, even if forming them raises the energy, provided this increase is below a certain threshold.

This latter type of model behaves as conjectured by Tlusty and Safran[27] one decade ago for understanding the critical behaviour of DHSs. The dipolar fluid was modelled as a thermodynamic ensemble of ideal (non-interacting) chains with two types of defects: free ends and Y- junctions. These authors concluded that the formation of ends promotes an effective repulsion between the particles, and the formation of junctions promotes an effective attraction. As the temperature is lowered, junctions and ends phase separate into a liquid rich in junctions, and a dilute vapour of chain ends. The Tlusty-Safran theory is notable because it (i) explains the unusual low temperatures and densities at which the DHS or DSS critical point is thought to be; (ii) offers a mechanism by which the critical point could disappear (when the energy cost of forming a chain end is less than three times the energy cost of forming a Y-junction); and (iii) predicts a re-entrant shape of the coexistence curve, with the density of the liquid phase decreasing as the temperature is lowered.

These theoretical predictions were recently (and for the first time) validated in a patchy particle model specifically designed to reproduce the physics of the Tlusty-Safran phase transition.[28] The characteristic re-entrant (or "pinched") phase diagram was calculated, and a study of the liquid and vapour phases revealed that Y-junctions and chain ends did indeed phase separate. The first-order perturbation theory of Wertheim (which, at low densities and temperatures, is equivalent to the Tlusty and Safran theory[25,28]) reproduces all the ingredients of the pinched phase diagrams.

The present manuscript extends our previous study, focusing on the phase behaviour as a function of the energy cost of forming a junction. The critical parameters (temperature and density) decrease as the energy cost of forming a junction increases, and the critical point disappears at a fixed value of this energy cost. Both the pinched phase diagram and the scaling of the critical parameters are shown to follow the predictions of Wertheim's thermodynamic first-order perturbation theory. The pinched phase coexistence is sustained by a balance between two contributions to the entropy: the higher entropy of junctions in the high-density phase compensates the lower entropy of chains in the same phase. We show that this balance is only possible, if the energy cost of forming a junction is below a certain threshold, at which the critical density and temperature vanish. Finally, we argue that the model represents an example of a system in which valence depends on temperature: the pinching behaviour is related to the decrease of the valence towards 2 along the liquid branch of the coexistence curve, as the temperature decreases.

The manuscript is organized as follows. In Sec. II, we describe our model in detail. In Sec. III, we give an account of the numerical methods employed: since the liquid-vapour phase transition occurs at low temperatures and densities (and more so as the energy cost of junctions increases), special numerical techniques had to be adopted. Section IV summarizes the theoretical methods employed in the present study and which are based on Wertheim's first-order perturbation theory. Results from both simulations and theory are presented in Sec. V. In Sec. VI, we comment on the analogies between our model and the phase behaviour of dipolar fluids. We summarize and conclude in Sec. VII. Appendix A goes into the details of the biased Monte Carlo (MC) moves employed in the simulations. Appendix B presents a table with the estimated numerical values of the coexistence properties of the model.

II. MODEL

We focus on a patchy particle model that self-assembles into chains connected by Y-junctions. It consists of hard spheres of diameter σ whose surface is decorated with patches of two types, A and B. Two patches of type A are placed on the poles, while nine patches of type B are equally spaced along the equator, as shown in Fig. 1.

The interaction energy $V_{ij,\alpha\beta}$ between patch α, belonging to particle i, and patch β, belonging to particle j, is given by the Kern-Frenkel potential.[29] Denoting by r_{ij} the vector joining the centres of particles i and j, $\hat{r}_{ij} = r_{ij}/|r_{ij}|$ and by $\hat{r}_{i\alpha}$ the unit vector from the centre of particle i to the centre of patch α on its surface, we have

$$V_{ij,\alpha\beta} = V_{\alpha\beta}^{SW}(|r_{ij}|) \times G(\hat{r}_{ij}, \hat{r}_{\alpha i}, \hat{r}_{\beta j}), \qquad (1)$$

where $V_{\alpha\beta}^{SW}$ is a square well potential,

$$V_{\alpha\beta}^{SW}(x) = \begin{cases} \infty & \text{if } x < \sigma, \\ -\epsilon_{\alpha\beta} & \text{if } \sigma < x < \sigma + \delta_{\alpha\beta}, \\ 0 & \text{otherwise,} \end{cases} \tag{2}$$

and G is the angle-dependent part,

$$G(\hat{r}_{ij}, \hat{r}_{i\alpha}, \hat{r}_{j\beta}) = \begin{cases} 1 & \text{if } \hat{r}_{ij} \cdot \hat{r}_{i\alpha} > \cos\theta_{\alpha\beta}^{max}, \\ & \text{and } -\hat{r}_{ij} \cdot \hat{r}_{j\beta} > \cos\theta_{\alpha\beta}^{max}, \\ 0 & \text{otherwise.} \end{cases} \tag{3}$$

The free parameters in the model are thus the interaction energies between patches $\epsilon_{\alpha\beta}$, their ranges $\delta_{\alpha\beta}$, and the angle $\theta_{\alpha\beta}^{max}$, the last two of which control the volume available for bonding. We shall henceforth take ϵ_{AA} as our unit of energy, and σ as our unit of length; all equations will, however, retain these parameters, for generality. It follows that all temperatures will be in units of ϵ_{AA}/k_B, where k_B is Boltzmann's constant.

In Secs. II A and II B, we provide a qualitative discussion of how the phase behaviour is affected by the choice of parameter values. Sections III–V are devoted to the quantitative study of this behaviour, as obtained from simulations and theory.

A. Energy scales of branching and chaining

We do not allow BB interactions and, therefore, we set $\epsilon_{BB} = 0$. This choice renders X-junctions impossible, leaving only AA interactions, which promote chain formation, and AB interactions, which yield Y-junctions. Setting $\epsilon_{BB} = 0$ leaves the ratio $r = \epsilon_{AB}/\epsilon_{AA}$ as the only parameter controlling the energy scales of chaining and branching. As we will show theoretically in Secs. IV–V, the ratio r is indeed the fundamental parameter governing the phase behaviour of the network fluid. By varying r we can in fact change the topology of the phase diagram. Let us now show why.

Given a system of linear AA chains, two types of defects can arise, as shown in Fig. 1. The first of these are chain ends, which consist of particles with one bonded and one unbonded A patch. The energy required to cut a chain along one of its AA bonds is ϵ_{AA}, and since this leads to the formation of two chain ends, the energy cost of a chain end is $\epsilon_e \equiv \epsilon_{AA}/2$. The second type of chain defects are Y-junctions, where a patch of type A binds to a patch of type B, thus providing a mechanism to connect two different chains. To form a junction, one first needs to create a chain end, whose energy cost is $\epsilon_{AA}/2$, and then connect this chain end to a B patch, with an energy gain of $-\epsilon_{AB}$: the energy cost of forming a junction is thus $\epsilon_j \equiv -\epsilon_{AB} + \epsilon_{AA}/2 = \epsilon_{AA}(1/2 - r)$.

The energy cost of forming a chain end is always positive, and, therefore, the ground state ($T = 0$) of the model does not contain any chain ends. On the other hand, the energy cost of forming junctions can be positive or negative, depending on the fundamental parameter $r = \epsilon_{AB}/\epsilon_{AA}$. If $r > 0.5$, the energy cost is negative, and, therefore, all possible Y-junction are present in the ground state. In this case, an ordinary liquid-vapour transition occurs.[25] On the other hand, if $r < 0.5$, then $\epsilon_j > 0$ and the ground state is characterized by the absence of Y-junctions (i.e., only AA bonds, or long – infinite – chains are present). Because linear chains do not phase separate, one could speculate that the same happens in our model for $r < 0.5$. However, chain defects (both ends and junctions) are always present at finite temperatures, and, therefore, the question arises of whether these defects are sufficient to drive a phase separation. Recently we provided an answer to this question,[28] by considering the case $r = 0.37$. Specifically, we showed that phase separation does occur between a high-density phase rich in junctions and a low-density phase rich in chain ends. Moreover, the binodal line exhibits a *pinched* shape, evidence that indeed the topological phase separation of Tlusty and Safran[27] is observed.

In the present manuscript, we will show that phase separation occurs only if $r > 1/3$. For $r < 1/3$, the energy cost of forming junctions is too high or, alternatively, the entropy gain is too small to offset the loss of translational entropy of chains in the liquid phase (a detailed discussion of this topic is given in Sec. V C).

B. Volume available for bonding

The parameters $\delta_{\alpha\beta}$ and $\theta_{\alpha\beta}^{max}$ determine the volume available for bonding, which in the Kern-Frenkel model can be written as

$$v_{\alpha\beta} = \frac{\pi\sigma^3}{3}[(1+\delta_{\alpha\beta})^3 - 1]\left[1 - \cos\left(\theta_{\alpha\beta}^{max}\right)\right]^2. \tag{4}$$

$v_{\alpha\beta}$ does not fix the topology of the phase diagram (i.e., whether a critical point exists or whether the phase diagram is pinched), only the density/temperature range where phase separation occurs.

We have chosen the set of parameters: $\delta_{AA} = 0.07$, $\delta_{AB} = 0.545$, $\cos(\theta_{AA}^{max}) = 0.98$, and $\cos(\theta_{AB}^{max}) = 0.9461856$, taking into account the following requirements:

- *single-bond-per-patch condition*, i.e., the patch interaction range must be small enough that a patch can be engaged in at most one bond. This condition is necessary in order to compare the simulation results with the predictions of Wertheim's first-order perturbation theory,[15,16] which rests on this assumption.
- large v_{AB}/v_{AA} ratio (where $v_{\alpha\beta}$ is the volume of an $\alpha\beta$ bond, defined more rigorously later). This condition is necessary in order to observe the pinched phase diagrams at temperatures accessible to simulations (for a theoretical discussion see Sec. IV). We have placed nine patches of type B to effectively increase v_{AB} without violating the *single-bond-per-patch condition*.

III. SIMULATION METHODS

A. Biased Monte Carlo moves

The interaction potential between two particles is strongly anisotropic and short-ranged. At low temperature the system is characterized by bonded configurations, which are notoriously difficult to sample. In fact, the phase space associated with bonded configurations is very small, and the standard Metropolis Monte Carlo algorithm has a low efficiency in locating them. Moreover, once a bonded

configuration is found, the underlying Markov chain is likely to get trapped due to the high-energy penalty of breaking bonds. At the lowest temperature studied, $T = 0.045$, for example, the probability of breaking a AA bond becomes of the order of $\exp(1/0.045)$, thus requiring $\approx 4 \times 10^9$ MC attempts to break such a bond.

To overcome this difficulty we implemented biased MC moves, inspired by the aggregation-volume-bias (AVB) MC Algorithm.[30] The idea behind these techniques is to preferentially place a particle into the bonding volume surrounding another particle and, conversely, to preferentially remove a bonded particle from the bonding region of its associated partner. The immediate advantage of this scheme is that bonded configurations are found much faster than with random sampling.

The bonding region is defined as the volume of phase space where another particle can form a bond according to the Kern potential previously defined. For an AA bond defined by the Kern potential in Eq. (1), this volume V_{AA} equals

$$V_{AA} = 4\pi {f_A}^2 v_{AA}, \tag{5}$$

where f_A is the number of A-type patches on each particle ($f_A = 2$ in our model), and v_{AA} is the bonding volume of an A *site*, given by Eq. (4).

Because we have $\epsilon_{AA} > \epsilon_{AB}$, AA bonds are always much stronger than AB bonds. We will therefore consider only biased moves inside V_{AA}, and leave the weaker AB bonds to the ordinary Metropolis moves (we have also run simulations with biased moves for AB bonds without any appreciable speed gain).

Two different types of biased moves are used in our simulations. The first type of bias is an implementation for patchy particles of the move described in Ref. 30, which is called an *AVB* move. The *AVB* move is not very effective at the lowest temperature considered in the present study. We have then designed a new biased move, which allows the different chains to effectively exchange particles at low temperatures, and which we call *End Hopping* move. Both moves are described in depth in the Appendix A.

In summary, a MC step comprises grand-canonical insertion/removal moves, bias moves, and ordinary Metropolis translational and rotational moves (the frequency of the moves is, respectively, 1:500:500).

B. Phase behaviour

To study the phase behaviour of the system we run successive umbrella sampling (SUS) MC simulations,[31] from which the full density probability, $P(\rho)$, can be extracted at fixed temperature T and chemical potential μ.

In the SUS method, the pertinent range $[0, N_{max}]$ of particles is divided into many small windows of size ΔN. For each window i, in the interval $N \in [N_i, N_i + \Delta N]$, a grand-canonical MC simulation is performed, avoiding the deletion or insertion of particles outside the window's range.[32] This allows the calculation of $H_i(N)$ which monitors how often a state with N particles is visited in the ith window. The full probability density $P(N)$ is then estimated recursively

$$\frac{P(N)}{P(0)} = \frac{H_0(1)}{H_0(0)} \cdots \frac{H_0(2)}{H_0(1)} \cdots \frac{H_0(\Delta N)}{H_0(\Delta N - 1)} \cdots \frac{H_i(N)}{H_i(N-1)}.$$

The free energy profile is calculated from $f(N) = -k_B T \log P(N) + cost.$

The advantages of the SUS method are manifold. The use of small windows allows an effective sampling of all the microstates without the use of biasing functions. Because the windows are independent, all the simulations can be run in parallel, with a speed gain which scales linearly with the number of processors. Once the full density probability has been obtained at fixed T and μ, histogram reweighting techniques[33] can be applied to obtain the density probability at different chemical potentials. Keeping track of the energy histogram during the SUS simulations allows also temperature reweighting. Histogram reweighting techniques are fundamental to locating both the critical point and the coexistence points.

Evaluation of the critical points starts with grand-canonical simulations searching for a temperature which displays critical-like density fluctuations. A SUS simulation is then run at such T, and the resulting density and energy histograms are reweighted until the best possible fit to the universal Ising distribution is obtained. We have not performed a finite-size study since we are only interested in the trends with varying r, but we have studied systems of different sizes L, up to $L = 25\,\sigma$.

The coexistence points at fixed T are obtained by reweighting the densities histogram until the two peaks (for the low- and high-density phases) have the same area and their average density provide precise estimates of the coexistence densities.

IV. THEORY

The theory of Wertheim,[15,16] developed in the context of associating fluids, provides a powerful tool for investigating, with parameter-free calculations, the thermodynamic properties of patchy particle models,[17,20,23] including models with dissimilar patches,[18,28] such as the present one. The quality of the theory is almost quantitative concerning the energy scale and semi-quantitative concerning the density scale.[17,20,23] One can therefore use the theoretical expressions to guide the design of the model as well as the choice of the relevant geometric parameters.

In Wertheim's approach, the free energy of a system with N particles is written as a sum of the reference hard sphere free energy (given by, e.g., the Carnahan-Starling form) and a bonding contribution,

$$\frac{\beta F_b}{N} = 2 \log X_A + f_B \log X_B - X_A - \frac{f_B}{2} X_B + \frac{1}{2}(2 + f_B), \tag{6}$$

where f_B is the number of B patches in each particle, $\beta \equiv (k_B T)^{-1}$, T is the temperature, and X_A and X_B are, respectively, the fractions of sites A and B which are not engaged in a bond. X_A and X_B can be related to temperature and density

through the laws of mass action,[25]

$$\begin{cases} X_A + 2\eta\Delta_{AA}X_A^2 + f_B\eta\Delta_{AB}X_AX_B = 1, \\ X_B + 2\eta\Delta_{AB}X_AX_B = 1, \end{cases} \tag{7}$$

where $\eta \equiv v_s\rho$ is the packing fraction, $v_s = \frac{\pi}{6}\sigma^3$ is the particle volume, ρ is the number density, and the quantities $\Delta_{\alpha\beta}$ ($\alpha, \beta = A, B$) are given by

$$\Delta_{\alpha\beta} = \frac{1}{v_s}\int g_{HS}(\mathbf{r})[\exp(\beta\epsilon_{\alpha\beta}) - 1]\, d\mathbf{r}, \tag{8}$$

where $g_{HS}(\mathbf{r})$ is the HS radial distribution function, and the integral extends over the bonding volume. The $\Delta_{\alpha\beta}$ are density dependent, via the density dependence of g_{HS}. If we consider a linear approximation for $g_{HS}(r)$,[34,35] then

$$\Delta_{\alpha\beta} = \bar{\Delta}_{\alpha\beta}g_{\alpha\beta}(\eta), \tag{9}$$

where

$$\bar{\Delta}_{\alpha\beta} = \frac{v_{\alpha\beta}}{v_s}[\exp(\beta\epsilon_{\alpha\beta}) - 1] \tag{10}$$

is density independent, and $v_{\alpha\beta}$ is the volume of an $\alpha\beta$ bond, given by Eq. (4). For our choice of parameters, $v_{AA}/v_s = 1.800344 \times 10^{-4}$ and $v_{AB}/v_s = 1.55685717 \times 10^{-2}$ so that the AA bonding volume is significantly smaller than the AB bonding volume.

The function $g_{\alpha\beta}$ that contains the η (packing fraction) dependence is

$$g_{\alpha\beta} = A_0(\eta) + A_1(\eta)x_{\alpha\beta}, \tag{11}$$

with

$$A_0 = \frac{1 - \eta/2}{(1-\eta)^3}, \tag{12}$$

$$A_1 = \frac{9}{2}\frac{\eta(1+\eta)}{(1-\eta)^3}. \tag{13}$$

Notice that $A_0(\eta)$ is the contact value of g_{HS}. The second term in Eq. (11) depends on the range $\delta_{\alpha\beta}$ of the square well of bond $\alpha\beta$:

$$x_{\alpha\beta} = 1 - \frac{3}{4}\frac{(1+\delta_{\alpha\beta})^4 - 1}{(1+\delta_{\alpha\beta})^3 - 1}. \tag{14}$$

In the limit of short ranges, i.e., when $\delta_{\alpha\beta} \to 0$, one has $x_{\alpha\beta} \to 0$ and $g_{\alpha\beta} \to A_0(\eta)$, as expected.

Differentiation of the free energy with respect to the volume yields the pressure, P. From the T and ρ dependencies of P one can locate, by standard methods, the critical point and the liquid-vapour coexistence curve. As shown below, for $r < 0.5$ the liquid-vapour binodal is re-entrant (or pinched): on cooling, the density of the coexisting liquid phase decreases, approaching the coexisting vapour density. This contrasts with the more usual behaviour that the densities of the two coexistence phases become more different as $T \to 0$, which is also found in the present model when $r > 0.5$.

A. Choice of the geometric parameters defining bonding

The dependencies of X_A and X_B on T help to understand the basic physics behind the pinching. Indeed, at high T, both X_A and X_B approach 1, since all sites are unbonded. At low

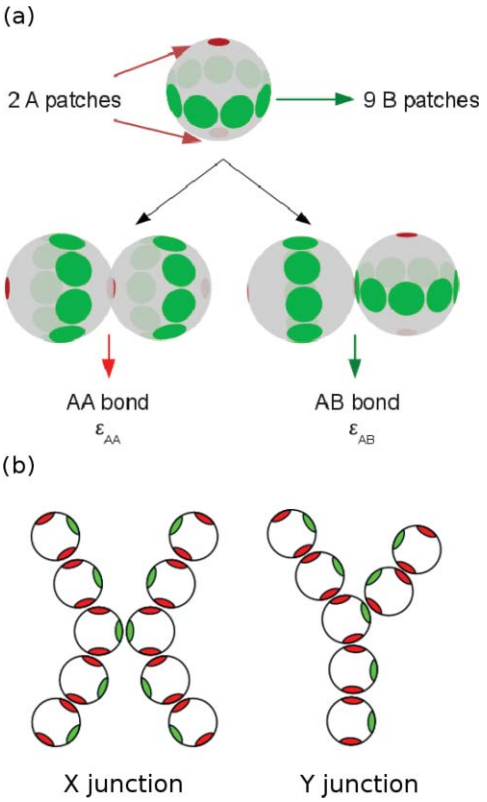

FIG. 1. (a) Schematic representation of the patchy particles. Two patches of type A are placed on the poles, while nine patches of type B are equally spaced along the equator. Two types of bonds are allowed: AA bonds, which are responsible for the formation of chains; and AB bonds, which form junctions connecting the different chains. (b) Schematic representation of a X-junction and a Y-junction. Only Y-junctions can form in our model since BB bonds are forbidden.

T, if $r < 0.5$, X_A approaches 0, since all A sites are bonded, whereas X_B again approaches 1. This behaviour can be understood by realizing that breaking two junctions (AB bonds) to form one AA bond (leaving the B sites unbonded) is energetically favourable ($\Delta E = +2\epsilon_{AB} - \epsilon_{AA} < 0$) when $r < 0.5$. X_B thus depends non-monotonically on T, as shown in Fig. 2 for a specific choice of the parameters. Hence, the number of junctions present in the system, $n_j = f_BN(1 - X_B)$, is also non-monotonic with T, being 0 both at high and low T. The maximum number of branching points depends on the smaller value assumed by X_B. As branching is a pre-requisite for the onset of a critical point,[36] it is important to select geometrical

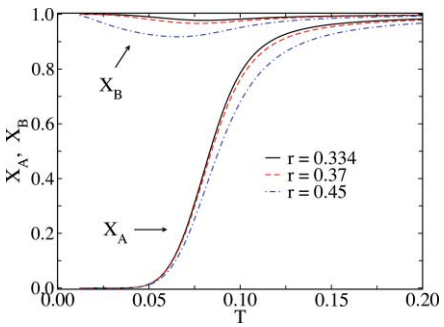

FIG. 2. Theoretical X_A and X_B *vs* T at $\rho = 0.05$, for three different r values. Note the non-monotonic behaviour of X_B.

parameters for bonding, such that a sufficient number of AB bonds develop in the T window where equilibrium numerical simulations are possible. Indeed, despite the significant speedup obtained by implementing the algorithms discussed in Sec. III A, a complete evaluation of the density of states is still limited to $T > 0.045$. Since the T-dependence of X_A and X_B is mostly controlled by the bonding volumes, we have chosen large values of V_{AB}/V_{AA} (i.e., small values of δ_{AA} and $\cos(\theta_{AB}^{max})$ and large values of δ_{AB} and $\cos(\theta_{AA}^{max})$), both still within the one-bond-per-patch limit.[37] For the same reason, we have chosen to work with $f_B = 9$. We stress that the choice of f_B and of the geometric parameters defining bonding does not alter the topology of the phase diagram (i.e., does not suppress or generate a critical point) but only the T-scale where condensation occurs. As we discuss in the following, the parameter that controls the presence of a critical point in the system is r, which does not depend on the bonding volumes.

B. Asymptotic expression for the bonding free energy in the strong-association limit

In this section, we rederive an asymptotic analytic expression for the bonding free energy in the strong-association limit, by generalizing the work in Refs. 25 and 26 to arbitrary f_B values and ρ-dependent $\Delta_{\alpha\beta}$. This extension is required to properly represent the low-T behaviour of the Wertheim free energy (Eq. (6)).

As in Ref. 25, we consider the bonding free energy $f_b \equiv F_b/N$ in the limit of strong AA association, i.e., $y \equiv (\eta\Delta_{AA})^{-\frac{1}{2}} \ll 1$, and in which we also have $r < 1$ or $\alpha \equiv (\Delta_{AB}/\Delta_{AA}) \ll 1$. We further consider $\alpha \sim y^2$. Under these hypotheses, the bonding free energy for the present patchy model can be expanded to first order in y, with the result (see also Eq. (34) of Ref. 25)

$$\beta f_b = 2\ln y - \sqrt{2}y - \sqrt{2}f_B\frac{\alpha}{y}. \tag{15}$$

This expression incorporates density-dependent $\Delta_{\alpha\beta}$ through the linear approximation for $g_{HS}(r)$, the key idea being that the appropriate expansion variable is α/y.

To obtain an asymptotic expression for the bonding contribution to the pressure, we proceed as follows: (i) calculate $\beta p_b v_s \equiv \eta^2(\partial\beta f_b/\partial\eta)$ and (ii) expand $p = p_{HS} + p_b$ to second order in η. The result reads

$$\beta p v_s = a_0\eta^{\frac{1}{2}} - a_1\eta^{\frac{3}{2}} + (B_2 - a_2)\eta^2, \tag{16}$$

where $B_2 = 4$ is the second virial coefficient of HSs (in units of the HS volume v_s), and

$$a_0 = \frac{1}{\sqrt{2\bar{\Delta}_{AA}}}, \tag{17}$$

$$a_1 = a_0\left(f\bar{\Delta}_{AB} - \frac{a_2}{2}\right), \tag{18}$$

$$a_2 = \frac{5}{2} + \frac{9}{2}x_{AA}. \tag{19}$$

By equating the first and second derivatives of the pressure (Eq. (16)) to zero, we obtain expressions for the critical point. After some manipulation, these can be rewritten as

$$\eta_c = \frac{a_{0,c}}{a_{1,c}} = \frac{1}{f_B\bar{\Delta}_{AB,c} - \frac{a_2}{2}}, \tag{20}$$

$$\left[f_B\bar{\Delta}_{AB,c} - \frac{a_2}{2}\right]^{\frac{3}{2}} = \bar{\Delta}_{AA,c}^{\frac{1}{2}}2\sqrt{2}(B_2 - a_2), \tag{21}$$

where the subscript c denotes quantities evaluated at the critical point. These expressions reduce to the asymptotic expressions of Ref. 25 (where a zero-density approximation for g_{HS}, viz., $g_{HS} = 1$, was used), if $a_2 = 0$. As we shall see later, it is important to account for the density dependence of g_{HS} to properly describe, with these asymptotic results, the theoretical predictions as well as the numerical MC data.

Interestingly enough, the conditions for the existence (or absence) of a critical point do not depend on a_2; hence, this improved expansion also confirms that no critical point exists when $r < 1/3$. Indeed, let us consider Eq. (21) in the low-temperature limit. In this limit, the -1 in Eq. (10) can be dropped, and $f\bar{\Delta}_{AB} \gg a_2/2$. Then, from Eq. (21), we have

$$k_B T_c = \frac{3\epsilon_{AB} - \epsilon_{AA}}{\ln C}, \tag{22}$$

with $C = 8(B_2 - a_2)^2 v_{AA} v_s^2/(f_B v_{AB})^3$. Hence $T_c > 0$, only if $3\epsilon_{AB} > \epsilon_{AA}$ ($r > 1/3$). In the same limit,

$$\ln\rho_c = -\beta_c\epsilon_{AB} - \ln f_B v_{AB}, \tag{23}$$

which provides a linear relation between $\ln\rho_c$ and $\frac{\epsilon_{AB}}{k_B T_c}$ (or, in other words, an exponential decrease of ρ_c with r). These equations for the critical parameters are the same as those of the Tlusty-Safran theory, which also predicts that there is no critical point for $r < 1/3$.

A comparison between the full solution of the Wertheim theory and the asymptotic expansion is presented in Fig. 3. It is important to notice that while T_c and ρ_c vanish at $r = 1/3$, T_c does so much more steeply than ρ_c. Thus, the (exponential) vanishing of ρ_c becomes more readily observable on decreasing r.

We can improve the above asymptotic results by including terms of order y^2 in the expansion (Eq. (15)). These terms

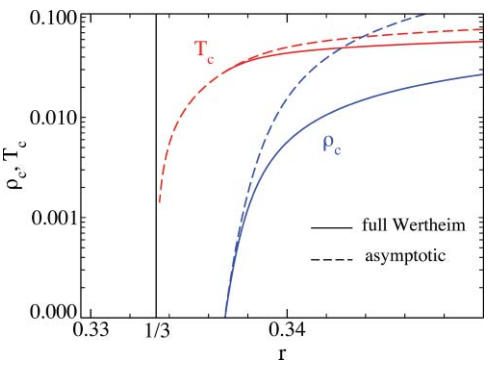

FIG. 3. Comparison of the critical parameters T_c and ρ_c from Wertheim theory (Eq. (6)) and from the asymptotic expressions (Eqs. (20) and (21)). Note the pronounced change in slope of the lines around $r = 1/3$.

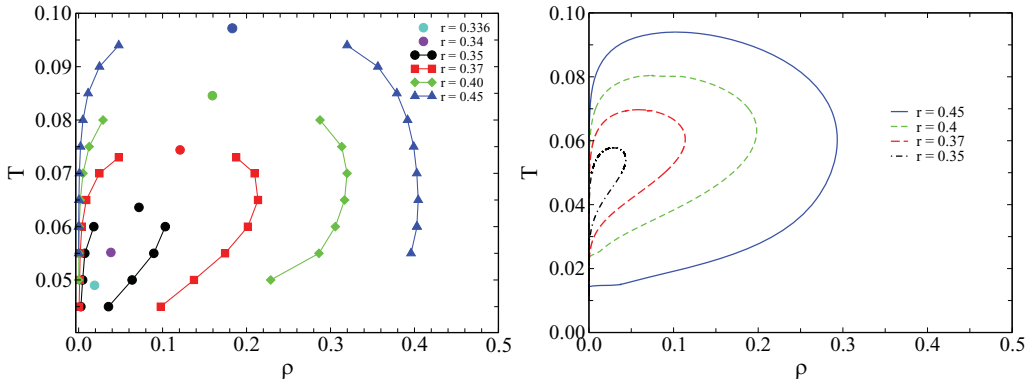

FIG. 4. Phase diagram of the model for several values of r. (a) Numerical MC data. (b) Theoretical predictions.

are

$$\beta f_{b,2} = \frac{y^2}{4} + \frac{f_B \alpha}{2} + \frac{f_B}{2}\left(\frac{f_B}{2} + 4\right)\left(\frac{\alpha}{y}\right)^2. \tag{24}$$

Proceeding as before to obtain their contribution to P, we conclude that they only affect the coefficient multiplying η^2:

$$\beta p_{b,2} v_s = \left[-\frac{9}{4} - 9x_{AA} + \frac{1}{2}a_2^2 + \frac{9 f_B \bar{\Delta}_{AB}}{2} \right. \tag{25}$$

$$\left. + f_B \bar{\Delta}_{AB}^2 \left(\frac{f_B}{2} + 4\right)\right] \frac{\eta^2}{2\bar{\Delta}_{AA}}. \tag{26}$$

Inclusion of this term in P improves only marginally the previous asymptotic expressions.

V. RESULTS

A. Phase diagram

As discussed in Sec. II, the energy cost of forming a junction is given by $\epsilon_j = \epsilon_{AA}(1/2 - r)$. We performed simulations at different values of r. The critical point was determined for $r = 0.336, 0.34, 0.35, 0.37, 0.40, 0.45$. The full phase diagram was calculated for $r = 0.35, 0.37, 0.40, 0.45$.

Results for the simulations are shown in Fig. 4(a), which displays several interesting features. We start by noting that for all r values a clear pinching is observed, which becomes more and more apparent on decreasing r towards 1/3. This pinching indicates that on cooling along a constant-density path that crosses the two-phase region, the system evolves from a homogeneous to a phase-separated to a homogeneous state again. We also note that, on decreasing r, both T_c and ρ_c decrease. Likewise, the liquid branch of the coexistence curve moves to lower densities. This is consistent with the progressive decrease in the amount of branching in the system, and bears strong resemblance to the drop in T_c and ρ_c observed in fluids of particles with identical patches on decreasing the average valence (i.e., the mean number of patches per particle). Consequently, empty liquids (i.e., liquids with vanishing densities[20]) can also form in the present system, for small r. As in the case of systems of fixed valence,[17] these liquid states consist of long chains of AA-bonded particles occasionally branching at the rare AB bonds, as shown in Fig. 5. The figure shows both the decrease of the density and the decrease in the number of junctions as the temperature is lowered from $T = 0.065$ to $T = 0.045$.

Figure 4(b) shows the corresponding coexistence curves calculated theoretically (Eq. (6)). As already found in previous patchy-particle models,[17,20] the theory correctly predicts the T-scale of the condensation, but significantly underestimates ρ_c and the density of the liquid-branch at coexistence.

The coexistence state points presented in Fig. 4 are also reported, for completeness, in Appendix B, which includes, in addition, the chemical potentials at coexistence and the sizes of the simulation box for all studied r values. As an illustrative example of the quality of the data obtained with the chosen MC methodology, we show in Fig. 6 the distribution of density fluctuations for the case $r = 0.35$ at $T = 0.55$, for several values of the activity z, encompassing the coexistence value. Distributions at different z are calculated via histogram reweighting.

B. Critical parameters

Figure 7 shows the r dependence of the critical parameters calculated from simulation and theory. Consistent with the preceding discussion, good agreement is observed for T_c, whereas ρ_c is underestimated. We note that, while ρ_c shows clear signs of vanishing at $\epsilon_{AB} \to 1/3$, the vanishing of T_c is less evident. On the other hand, comparison with the

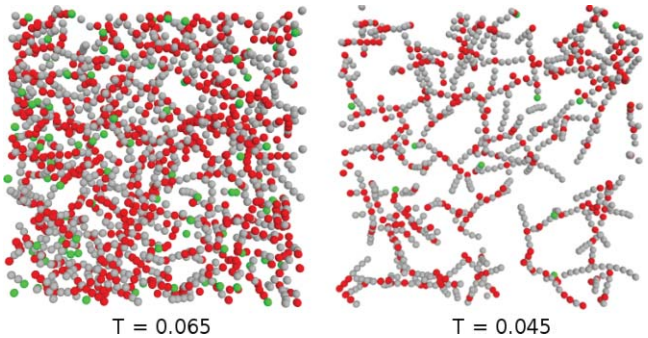

FIG. 5. Projection of two slabs of thickness 5σ of the liquid at coexistence at $T = 0.065$ (left) and $T = 0.045$ (right), for $r = 0.37$. The edge length of the simulation box is, respectively, 36σ and 45σ. Silver particles are chain particles, red particles are junctions, and green particles are chain ends. Note that the low-T system has a lower density than the high-T system, due to the retracing of the phase diagram.

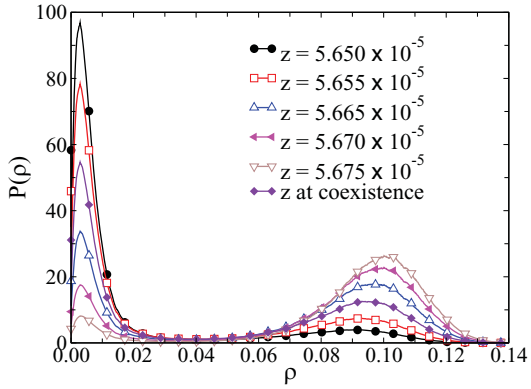

FIG. 6. Distribution of the density fluctuations for $r = 0.35$, $T = 0.55$, and several values of the activity z, including that at coexistence, $z = 5.66 \times 10^{-5}$.

theoretical predictions shows that indeed T_c starts to show clear signatures of approaching 0 only when ϵ_{AB} is very close to $1/3$.

To strengthen the evidence for vanishing T_c on approaching $r = 1/3$, we proceed to compare ϵ_{AB}/T_c and $\ln \rho_c$, in the form predicted by Eq. (23). These can be calculated either from the full Wertheim theory, or from the asymptotic relations (the latter by combining Eqs. (20) and (21)). Figure 8 shows the resulting ϵ_{AB}/T_c *vs* $\ln \rho_c$ plot: the theoretically expected proportionality $\ln \rho_c \propto \epsilon_{AB}/T_c$ indeed holds, but the y intercept is not very well predicted. If indeed $\ln \rho_c \propto \epsilon_{AB}/T_c$, then T_c also vanishes as $\rho_c \to 0$ (a limit where Wertheim's theory is exact).

C. Structure and thermodynamics at coexistence

The significant agreement between theoretical and numerical results strongly suggests that the theory may shed further light on some special features responsible for, or associated with, the pinching phenomenon.

Figure 9 shows the mean number of bonded sites per particle along the coexistence curve, evaluated from theory for several values of r. The figure is very illuminating since it shows that the number of connections per particle always approaches 2 at low T, confirming that the lowest energy state

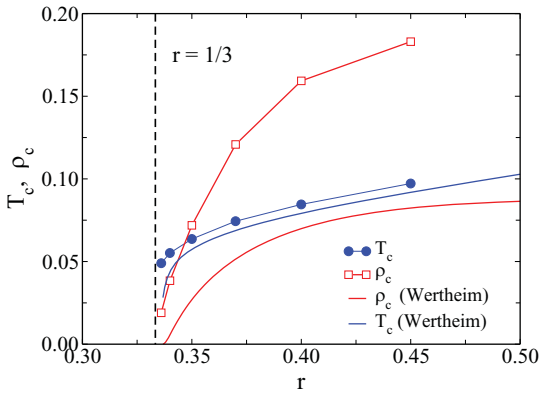

FIG. 7. Comparison between theory and simulation for the r dependence of the critical parameters.

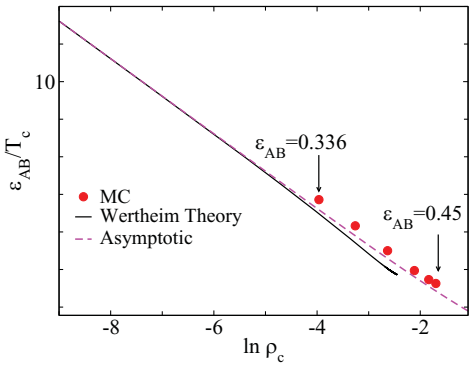

FIG. 8. Relation between T_c and ρ_c from simulations (symbols) and from theory (lines). Equation (23) predicts $\epsilon_{AB}/T_c = 2.56 - \ln \rho$.

of the system is composed of infinite chains (or closed loops) of bonded particles. The progressive decrease of the number of branching points on cooling forces the system to organize itself, in the liquid branch, into longer and longer chains connected by a smaller and smaller number of branching points. In this way, lower and lower average densities are generated. Figure 9 is also illuminating on the reasons behind the disappearance of the critical point when $r \to 1/3$. Indeed, on decreasing r the mean number of bonded sites per particle approaches 2 both in the vapour and liquid phases.

In Fig. 10, we plot the differences in entropy per particle, $\Delta s = s_l - s_v$, and internal energy per particle, $\Delta u = u_l - u_v$, between the liquid and vapour phases, as functions of T, for $r = 0.37$. As in an ordinary condensation, this balance is such that the lower entropy of the liquid phase is compensated by its lower energy. This result would seem to contradict the interpretation of the phase transition proposed in Refs. 27 and 38. According to these authors, the mechanism driving phase coexistence is that the loss of translational entropy of the chains (lower in the denser phase) is offset by the increase of the entropy of the self-assembled junctions (higher in the denser phase).

In order to clarify this point, we present a brief analysis of phase separation in terms of the entropy and internal energy differences between the coexisting phases. At a given pressure and temperature, the coexistence between two

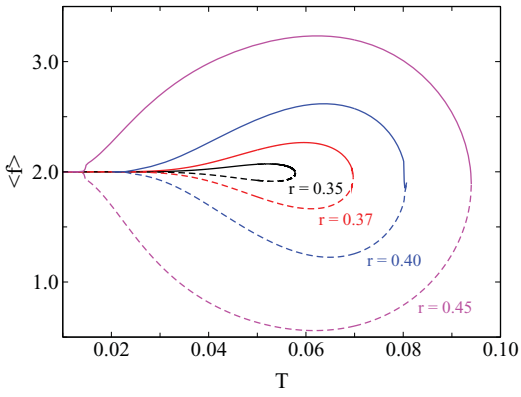

FIG. 9. Mean number of bonded sites per particle along the binodal line, calculated from Wertheim's theory. Full lines represent the liquid branch, and dashed lines represent the vapour branch.

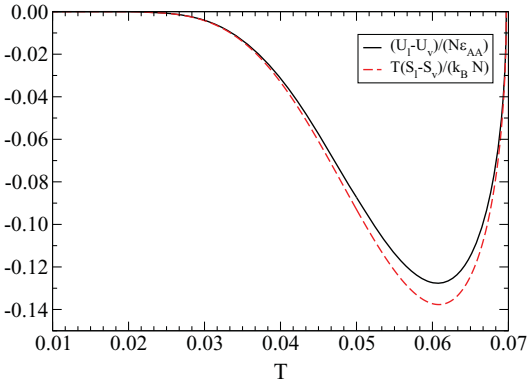

FIG. 10. Differences in entropy $S_v - S_l$ and internal energy $U_v - U_l$ between the liquid and vapour phases along the coexistence curve.

phases is expressed by the equality of their chemical potentials $\mu \equiv (\partial(f\eta)/\partial\eta)$, where η is the packing fraction and $f = u - Ts$ is the free energy per particle. We thus have

$$\mu = u - Ts + \eta\left(\frac{\partial u}{\partial \eta} - T\frac{\partial s}{\partial \eta}\right),$$

and the coexistence condition ($\Delta\mu = 0$) becomes

$$\Delta u - T\Delta s + \Delta\left(\eta\frac{\partial u}{\partial \eta}\right) - T\Delta\left(\eta\frac{\partial s}{\partial \eta}\right) = 0, \tag{27}$$

where $\Delta Z = Z_l - Z_v$ is the difference between the liquid- and vapour-phase values of any quantity Z. Expressions for u and s can be obtained by noting that $u = -\epsilon_{AA}(1 - X_A) + f_B(1 - X_B)(\epsilon_{AA}/2 - \epsilon_{AB})$ and using Wertheim's (Eq. (6)) and HS contributions to the free energy. In order to isolate each individual contribution (from chains and junctions) to the entropy and the internal energy, we derive asymptotic expressions for these quantities, in the same limit and to the same order of approximation used to arrive at Eqs. (15) and (16). This calculation shows that, at low densities and for strong AA association, the free energy difference between phases contains entropic contributions only:

$$\Delta u - T\Delta s = -k_B T(\Delta s_{ch} + \Delta s_{HS} + \Delta s_Y), \tag{28}$$

with $s_{ch} = 2a_0\eta^{-\frac{1}{2}}$, $s_{HS} = -(B_2 - a_2)\eta$, and $s_Y = 2a_1\eta^{\frac{1}{2}}$, and coefficients a_0, a_1, and a_2 given by Eqs. (17)–(19), respectively. These terms have the following physical meaning: s_{ch} is the translational entropy of chains, s_Y is the entropy of junctions, while s_{HS} is the entropy due to the excluded volume of the hard cores. Note that the same functional dependence of the entropy terms was assumed by Tlusty and Safran[27] based on mean-field arguments, while here it is rigorously derived from first principles. This equation reveals that, at the lowest order of Eqs. (15) and (16), the change in internal energy on going from the vapour into the liquid phase is cancelled by some part of the change in entropy. Therefore, the terms in the right-hand side of Eq. (28) represent the entropy variation that is relevant for phase coexistence. s_{ch} and s_{HS} are associated with chains, and $\Delta s_{ch} < 0$, $\Delta s_{HS} < 0$, i.e., chains contribute an entropy loss upon condensation. On the other hand, s_Y is the entropy of junctions and $\Delta s_Y > 0$, so Y-junctions contribute an entropy gain as the vapour turns into liquid at coexistence. Differentiating Eq. (28) with respect to η and substituting the results in Eq. (27), the following necessary condition for coexistence is obtained:

$$2\Delta s_{HS} + \frac{1}{2}\Delta s_{ch} + \frac{3}{2}\Delta s_Y = 0. \tag{29}$$

This equation clarifies the claim made in Refs. 27 and 38 that the entropy loss of the chains must be balanced by an entropic gain of the junctions. Moreover, Eq. (29) provides a physical interpretation for the absence of phase separation when $r < 1/3$. In fact, by taking the limit $\Delta\eta \to 0$ in Eq. (29), one can show that $\eta(\partial p v_s/\partial\eta) = 0$ is a necessary condition for that equality to hold. Then, by repeating the analysis of the critical point performed in Sec. IV B, it is found that Eq. (29) only has solutions when $r > 1/3$. Therefore, when $r \leq 1/3$, the gain in entropy of junction formation cannot overcome the entropy loss associated with chains, and the critical point vanishes.

VI. ANALOGIES WITH DIPOLAR FLUIDS

An important class of systems where particle aggregation couples with phase separation is dipolar fluids. Many studies[9,10] have confirmed that at low densities and temperatures, the strong anisotropy of the dipolar interaction favours the formation of linear chains and branched structures. Even though the dipolar interaction is long-ranged (with its r^{-3} decay), it was shown that, in the absence of external magnetic fields, a thermodynamic limit exists[39] and the interaction becomes "nearly short-ranged" for one-dimensional objects.[27] Based on this assumption, Tlusty and Safran[27] have developed a theory for the condensation of dipolar fluids. It is an example of hierarchical phase transition, where the entities involved in the phase separation process are not the individual dipoles, but the *equilibrium polymers* into which they aggregate.

We have shown in Secs. I–V that our model has many analogies with the Tlusty-Safran model for dipolar fluids, in particular:

- it accounts for the aggregation of particles into chains connected by Y-junctions;
- it can have (or not) a critical point, depending on the relation between the energy scales of branching and chaining;
- when a critical point exists, it exhibits a re-entrant (or *pinched*) phase diagram;
- in the limit of strong association, its free energy reduces to that of the Tlusty-Safran model.

In addition to correctly capturing the physics of the TS transition, our model has some relevant advantages. First of all, it is a microscopic model, and not a coarse-grained one. Its properties can be computed with powerful liquid-state theories, showing that a complete description of these systems can be achieved through rigorous statistical mechanics. Furthermore, the model is simple enough for its properties to be fully accessible with present-day computer simulation techniques and resources (unlike DHSs or DSSs).

Let us take as an example the DHS or DSS fluids, where the point dipole is embedded, respectively, in hard- and soft-sphere particles. If we imagine that our model indeed captures the physical mechanisms underlying the phase transition in DHSs or DSSs, the following predictions may be made, on the basis of the present study:

- DHSs or DSSs will display a critical point or not, depending on the energy cost of forming junctions. The long range of the interaction does play an important role in determining this energy cost. Indeed, simulations have shown that truncating the dipolar interactions appears to give rise to a phase transition,[40,41] whereas using the Ewald summation seems to suppress the transition.[10]
- The vanishing of the critical parameters is highly nonlinear, as shown in Fig. 7. Approaching the limiting value $r = 1/3$ below which there is no critical point, a strong suppression of the critical density will occur, with the critical temperature dropping to 0 only very close to $r = 1/3$. This result casts doubts on previous attempts at locating the DHS critical point by extrapolating to the DHS limit in systems where the cost of defects is much less than for DHS. See also Ref. 11 and references therein.

VII. CONCLUSIONS

In this article, we have introduced a specific model which, as predicted by Wertheim's theory and verified by numerical simulations, exhibits a novel type of liquid-vapour coexistence, i.e., a re-entrant (or pinched) phase diagram. This model is based on the idea of dissimilar-patch colloids introduced in Refs. 25 and 26, i.e., patchy colloidal particles with patches of different types (A and B in the present case), differing in their bonding energy and bonding volumes. The model has been optimized to bring the expected novel behaviour into the numerically accessible T-window. This has been achieved by an appropriate choice of the bonding volume of the AB interactions and of the number of B patches, to entropically favour the formation of AB bonds over AA bonds. Colloids of this type can in principle be fabricated by a selective functionalization of specific areas of the particles.[42–45]

Models with dissimilar patches significantly expand over models with identical patches.[17,20,23] Both types of models share the physics of a limited number of patches, the possibility of generating liquid states of vanishingly low densities (empty liquids), and the potential to give rise to equilibrium gels.[21] In addition, dissimilar-patch models benefit from the ability to control the effective valence through an accurate choice of T. Because we are able to tune the concentration of branching points by adjusting r and T, it becomes possible to suppress completely the liquid-vapour critical point (the case in which $r < 1/3$); or to generate a re-entrant phase diagram (the case investigated in this article, $1/3 < r < 1/2$); or, alternatively, to generate the standard behaviour where branching remains dominant also at low T (the case investigated in Ref. 18 $r > 0.5$).

The results reported in this article show that the designed model is indeed characterized by a pinched phase diagram. MC simulations, with specific acceptance and rejection moves, have confirmed the theoretical predictions, not only on the re-entrant shape of the coexistence curve, but, more importantly, on its variation with r. On decreasing r the coexistence region shrinks and appears to vanish when $r \to 1/3$, in full agreement with the theoretical predictions. The progressive suppression (down to full disappearance) of the liquid-vapour critical point is shown to be associated with a vanishing of the critical parameters. Interestingly, both theory and simulations show that while ρ_c depends strongly on r, T_c decreases rather smoothly, and only in a very small range of r close to $1/3$, it falls sharply towards 0.

As discussed in Sec. I, the thermodynamics of the present model is analogous to that proposed almost a decade ago by Tlusty and Safran[27,38] for several network aggregates, including DHS (Refs. 46–51) and telechelic micelles. The Tlusty and Safran model focuses on two types of topological defects of the network fluid, namely, chain ends and branching points (Y-junctions), and the phase transition results from the competition between a low-density phase, rich in chain ends, and a high-density phase, rich in junctions. Our model thus provides a microscopic off-lattice realization of the Tlusty and Safran mechanism,[27] where the chains, chain ends, and junctions emerge at low T, as strong many-particle correlations. As shown in Refs. 25 and 26, a precise mapping between the energetic cost of chain ends and chain junctions in Tlusty and Safran's model and ϵ_{AB} and ϵ_{AA} in our model can be provided. The connection between our model and the DHS or DSS fluids suggests that whether DHSs (or DSSs) have a critical point or not may depend on a rather delicate balance between the cost of creating a junction and the cost of creating a chain end. In this respect, the difficulty in locating T_c in all models which have the DHS fluid as their limit[10,52,53] strongly resembles the sudden crossover found in our model, from a linear decrease to a fast approach to 0, very close to $r = 1/3$.

We note how the present model also sheds light on the onset of liquid-vapour criticality in simple systems. In fluids where particles interact via spherically symmetric potentials (excluded volume plus monotonic attraction), a (stable or metastable) liquid-vapour critical point always exists and the range and strength of the interaction only controls the value of T_c. In patchy particles,[14] the existence of a critical point depends sensitively on the number and geometry of the patches themselves. Besides attraction, criticality depends on the possibility of forming a percolating structure of bonded particles. The present model adds a new piece of information, by clarifying that branching (i.e., the ability to form a three-dimensional spanning network) is not a sufficient condition for criticality. The formation of closed-bonded clusters (bond rings, micelles, and vesicles) can suppress the standard liquid-vapour critical point, giving rise to systems where self-assembly is the dominant[2,3,54] (and often only) aggregation phenomenon.[55–58]

We stress that the basic physics underlying the pinching behaviour can be understood in terms of the dependence of the critical parameters $T_c(f)$ and $\rho_c(f)$ on the particle

valence f. In the case of patchy particles with fixed valence (i.e., f identical bonding sites), the width of the phase diagram (the difference between coexisting liquid and vapour densities) vanishes as $f \to 2^+$. Hence, for any f value larger than 2, a critical point at finite T and ρ exists. In the present system, on cooling, more and more bonds are formed, many of them of the AB type, generating ramified connections between distinct particles and, if $1/3 < r < 1/2$, the emergence of a critical point. However, whereas when all patches are identical the number of branching points progressively increases on further cooling, as more and more bonds are formed, in the case of dissimilar patches, more efficient (in terms of energy) bonding will be achieved by progressively switching from AB bonds to AA bonds. This decrease in the number of junctions n_j on cooling is effectively equivalent to a reduction of the average valence of the system and, in the language of the identical-patches model, to a progressive decrease of the density of the coexisting liquid. Thus, T controls the effective valence and drives the pinching process.

We conclude by pointing out that the present model is amenable to direct experimental verification, through recent advances in colloidal synthesis. Two approaches appear particularly promising. One possibility is the use of triblock colloidal particles[59,60] which consist of spheres where the poles and the equator can be independently functionalized, allowing both for the chaining of particles and the formation of Y-junctions. Another possibility is the use of DNA constructs or colloidal particles functionalized with complementary DNA strands,[61] where interactions equivalent to our AA and AB bonds can be obtained by tuning the length, number, and sequence of the strands.

ACKNOWLEDGMENTS

We thank P. J. Camp for valuable comments and discussions. J. R. and F. S. acknowledge support from ERC-226207-PATCHYCOLLOIDS and ITN-234810-COMPLOIDS. J.M.T., P.I.C.T., and M.M.T.G. acknowledge financial supports from the Foundation of the Faculty of Sciences of the University of Lisbon and FCT (Contract Nos. POCTI/ISFL/2/618 and PTDC/FIS/098254/2008).

APPENDIX A: BIASED MONTE CARLO MOVES

We give here a detailed account of the MC biased moves used in the simulations. The difficulty in simulating network fluids at low temperatures is due to the bonded configurations of particles, whose sampling requires many chain-forming and chain-breaking events. Chain-forming events are rare since the volume in phase space of bonded configurations is much smaller than the total volume available. On the other hand, chain breaking is a rare process owing to the Boltzmann penalty that such events face.

The idea behind biased sampling is to enhance the acceptance probability, $acc(o \to n)$, for going from state o to state n of the MC chain by using a non-symmetric transition probability matrix, $\alpha(o \to n)$

$$\frac{acc(o \to n)}{acc(n \to o)} = \frac{\alpha(n \to o)}{\alpha(o \to n)} \exp(-\beta \Delta U).$$

In what follows we describe two different types of biased move: the "AVB move" which was introduced in Ref. 30, and the "end hopping move" which we introduce for the first time in the present study. Both moves enhance bond formation by directly placing particles inside the bonding volume, but address the bond-breaking issue in different ways. The "AVB" move uses the large ratio between the total volume and the bonding volume to effectively enhance the chain breaking probability. The "end hopping" move instead circumvents the penalty associated with the Boltzmann factor altogether by attempting moves that do not change the overall energy of the system.

1. AVB move

The AVB move enhances bond formation by directly placing particles inside the bonding volume, and takes advantage of the large ratio between the total volume and the bonding volume effectively to enhance the chain-breaking probability.

The AVB move comprises two types of moves, the bonding move and the unbonding move. The first of these takes a particle and places it inside the bonding volume of another particle. The second takes a particle and places it outside the bonding volume of one of its interacting neighbours. In the following scheme we provide the details of the move. The quantity in parentheses at the end of each step indicates the probability associated with the trial move ($\alpha(o \to n)$), which is accounted for in the acceptance probability.

- Choose between bonding or unbonding move $(1/2)$
  - (1) Bonding move
    - (a) select a particle i, bonded with N_i other particles $(1/N)$;
    - (b) select a particle j outside the bonding volume of particle i $(1/(N - N_i - 1))$;
    - (c) place particle j inside the bonding volume of particle i $(1/V_{AA})$. Note that particle j has to be placed uniformly inside V_{AA} (for example, placing the centre of mass of particle j around a randomly selected patch of particle i, and randomly selecting an orientation for which particles i and j interact);
    - (d) accept move with probability

$$acc(\text{bond}) = \frac{(N - N_i - 1)V_{AA}}{(N_i + 1)(4\pi V - V_{AA})} \times \exp(-\beta \Delta E).$$

  - (2) Unbonding move
    - (a) select a particle i $(1/N)$;
    - (b) select a particle j inside the bonding volume of particle i $(1/N_i)$;

(c) place particle j outside the bonding volume of particle i $(1/(4\pi V - V_{AA}))$;
(d) accept move with probability

$$acc(\text{unbond}) = \frac{N_i(4\pi V - V_{AA})}{(N - N_i)V_{AA}} \times \exp(-\beta \Delta E).$$

Care must be taken to insert the particles uniformly into the bonding volume.

The great advantage of this scheme is that the acceptance ratio of the unbonding move contains a new term which favours the breaking of bonds ($\propto V/V_{AA}$) despite the strong energy penalty ($\exp(-\beta\Delta E)$).

2. End hopping move

At very low temperatures the Boltzmann factor associated with the energy penalty of breaking a bond completely suppresses the acceptance probability of the unbonding move. To solve this sampling problem, we introduce here the *end hopping* move, which generates trial moves that leave the energy unchanged. The move proceeds by selecting randomly a chain end, i.e., a particle which is engaged in only one AA bond, and moving it into the bonding volume of another chain end or of a monomer. Because the move leaves the number of bonds unchanged, its energy cost is null, and, therefore, it is cost-effective at any temperature (provided that chain ends exist in the simulation box). This move allows different chains to exchange particles, and allows efficient exploration of configurations with equal energy.

We provide here the details of the algorithm with the trial probabilities in parentheses after each step.

- Select a particle i which is also a chain end $(1/N_{\text{ends}})$;
- select a target particle j which is either a chain end different from i, or a monomer $(1/(N_{\text{ends}} + N_{\text{mon}} - 1))$;
- place particle i in the free bonding volume of particle j $(2/V_{AA}$, if j is a chain end; $1/V_{AA}$, if j is a monomer);
- if after the move particle i is not a chain end, reject the move;
- accept the move with probability

$$acc(\text{cee}) = \frac{N_{\text{end}}(N_{\text{end}} + N_{\text{mon}} - 1)}{(N^*_{\text{end}} + N^*_{\text{mon}} - 1)(N^*_{\text{end}})} \times \frac{1 + \delta_{\text{mon}}}{1 + \delta^*_{\text{mon}}} \exp(-\beta \Delta E),$$

where N^*_{end} and N^*_{mon} are, respectively, the number of ends and the number of monomers in the reverse move, and $\delta_{\text{mon}} = 1\,(0)$, if the target particle in the direct move is a monomer (end) (δ^*_{mon} is the same quantity for the reverse move).

APPENDIX B: COEXISTENCE PROPERTIES

The following table reports the numerical values of the excess chemical potential μ_{ex}, the coexisting densities ρ_{low} and ρ_{high}, and the simulated box size L, for $r = 0.35, 0.37, 0.40, 0.45$. The relative error on ρ_{low} and ρ_{high} is of the order of a few percent.

T	μ_{ex}	ρ_{low}	ρ_{high}	L
		$r = 0.35$		
0.0636	−0.4762	0.03935	0.104	24
0.0600	−0.5013	0.01808	0.103	20
0.0550	−0.5379	0.00736	0.090	22
0.0500	−0.5764	0.00478	0.064	24
0.0450	−0.6163	0.00266	0.036	28
		$r = 0.37$		
0.0738	−0.4221	0.059	0.175	18
0.0730	−0.4266	0.048	0.187	14
0.0700	−0.4443	0.025	0.210	14
0.0650	−0.4755	0.0091	0.214	14
0.0600	−0.5086	0.0038	0.202	14
0.0550	−0.5436	0.0019	0.175	14
0.0500	−0.5805	0.0012	0.137	14
0.0450	−0.6190	0.0006	0.098	18
		$r = 0.40$		
0.0835	−0.3961	0.0658	0.237	16
0.0800	−0.4131	0.0290	0.287	16
0.0750	−0.4395	0.0126	0.313	16
0.0700	−0.4674	0.0051	0.320	16
0.0650	−0.4968	0.0020	0.317	16
0.0600	−0.5276	0.00072	0.306	16
0.0550	−0.5597	0.00029	0.286	16
0.0500	−0.5920	8.66×10^{-5}	0.229	17
		$r = 0.45$		
0.0970	−0.3964	0.1128	0.253	16
0.0940	−0.4092	0.0478	0.320	16
0.0900	−0.4271	0.0248	0.356	16
0.0850	−0.4506	0.0113	0.379	16
0.0800	−0.4752	0.0051	0.392	16
0.0750	−0.5009	0.0022	0.399	16
0.0700	−0.5274	0.00090	0.403	16
0.0650	−0.5546	0.00032	0.404	16
0.0600	−0.5828	9.91×10^{-5}	0.403	16
0.0550	−0.6109	2.54×10^{-5}	0.396	15

[1] A. Walther and H. Müller, Soft Matter **4**, 663 (2008).
[2] F. Sciortino, A. Giacometti, and G. Pastore, Phys. Rev. Lett. **103**, 237801 (2009).
[3] A. Reinhardt, A. J. Williamson, J. P. K. Doye, J. Carrete, L. M. Varela, and A. A. Louis, J. Chem. Phys. **134**, 104905 (2011).
[4] V. F. Puntes, K. M. Krishnan, and A. P. Alivisatos, Science **291**, 2115 (2001).
[5] K. Butter, P. H. H. Bomans, P. M. Frederik, G. J. Vroege, and A. P. Philipse, Nature Mater. **2**, 88 (2003).
[6] M. Klokkenburg, R. P. A. Dullens, W. K. Kegel, B. H. Erné, and A. P. Philipse, Phys. Rev. Lett. **96**, 037203 (2006).
[7] J. Dudowicz, K. F. Freed, and J. F. Douglas, Phys. Rev. Lett. **92**, 045502 (2004).
[8] J. Stambaugh, K. van Workum, J. F. Douglas, and W. Losert, Phys. Rev. E **72**, 031301 (2005).
[9] P. J. Camp, J. C. Shelley, and G. N. Patey, Phys. Rev. Lett. **84**, 115 (2000).
[10] G. Ganzenmüller, G. N. Patey, and P. J. Camp, Mol. Phys. **107**, 403 (2009).
[11] R. Jia, H. Braun, and R. Hentschke, Phys. Rev. E **82**, 062501 (2010).
[12] S. C. Glotzer and M. J. Solomon, Nature Mater. **6**, 557 (2007).
[13] A. B. Pawar and I. Kretzschmar, Macromol. Rapid Commun. **31**, 150 (2010).
[14] E. Bianchi, R. Blaak, and C. Likos, Phys. Chem. Chem. Phys. **13**, 6397 (2011).

[15]M. Wertheim, J. Stat. Phys. **35**, 19 (1984); **35** (1984).
[16]M. Wertheim, J. Stat. Phys. **42**, 459 (1986); **477** (1986).
[17]E. Bianchi, P. Tartaglia, E. La Nave, and F. Sciortino, J. Phys. Chem. B **111**, 11765 (2007).
[18]J. M. Tavares, P. I. C. Teixeira, M. M.T. da Gama, and F. Sciortino, J. Chem. Phys. **132**, 234502 (2010).
[19]E. Zaccarelli, S. V. Buldyrev, E. La Nave, A. J. Moreno, Saika-Voivod, F. Sciortino, and P. Tartaglia, Phys. Rev. Lett. **94**, 218301 (2005).
[20]E. Bianchi, J. Largo, P. Tartaglia, E. Zaccarelli, and F. Sciortino, Phys. Rev. Lett. **97**, 168301 (2006).
[21]B. Ruzicka, E. Zaccarelli, L. Zulian, R. Angelini, M. Sztucki, A. Moussaïd, T. Narayanan, and F. Sciortino, Nature Mater. **10**, 56 (2011).
[22]E. Zaccarelli, J. Phys.: Condens. Matter **19**, 323101 (2007).
[23]J. Russo, P. Tartaglia, and F. Sciortino, J. Chem. Phys. **131**, 014504 (2009).
[24]J. Russo and F. Sciortino, Phys. Rev. Lett. **104**, 195701 (2010).
[25]J. M. Tavares, P. I. C. Teixeira, and M. M. Telo da Gama, Phys. Rev. E **80**, 021506 (2009).
[26]J. M. Tavares, P. I. C. Teixeira, and M. M. Telo da Gama, Mol. Phys. **107**, 453 (2009).
[27]T. Tlusty and S. A. Safran, Science **290**, 1328 (2000).
[28]J. Russo, J. M. Tavares, P. I. C. Teixeira, M. M. Telo da Gama, and F. Sciortino, Phys. Rev. Lett. **106**, 085703 (2011).
[29]N. Kern and D. Frenkel, J. Chem. Phys. **118**, 9882 (2003).
[30]B. Chen and J. I. Siepmann, J. Phys. Chem. B **105**, 11275 (2001).
[31]P. Virnau and M. Müller, J. Chem. Phys. **120**, 10925 (2004).
[32]B. J. Schulz, K. Binder, M. Müller, and D. P. Landau, Phys. Rev. E **67**, 067102 (2003).
[33]A. M. Ferrenberg and R. H. Swendsen, Phys. Rev. Lett. **63**, 1195 (1989).
[34]I. Nezbeda and G. Iglesia-Silva, Mol. Phys. **69**, 767 (1990).
[35]F. Sciortino, E. Bianchi, J. F. Douglas, and P. Tartaglia, J. Chem. Phys. **126**, 4903 (2007).
[36]A. F. A. Coniglio, U. De Angelis, and G. Lauro, J. Phys. A **10**, 219 (1977).
[37]F. Romano, E. Sanz, and F. Sciortino, J. Phys. Chem. B **113**, 15133 (2009).
[38]A. Zilman, T. Tlusty, and S. A. Safran, J. Phys.: Condens. Matter **15**, 57 (2003).
[39]S. Banerjee, R. B. Griffiths, and M. Widom, J. Stat. Phys. **93**, 109 (1998).
[40]K. Ng, J. P. Valleau, G. M. Torrie, and G. N. Patey, Mol. Phys. **38**, 781 (1979).
[41]P. J. Camp, private communication (2011).
[42]D. J. Kraft, J. Groenewold, and W. K. Kegel, Soft Matter **5**, 3823 (2009).
[43]Y.-S. Cho, G.-R. Yi, J.-M. Lim, S.-H. Kim, V. N. Manoharan, D. J. Pine, and S.-M. Yang, J. Am. Chem. Soc. **127**, 15968 (2005).
[44]A. B. Pawar and I. Kretzschmar, Langmuir **24**, 355 (2008).
[45]Q. Chen, S. C. Bae, and S. Granick, Nature (London) **469**, 381 (2011).
[46]P. G. de Gennes and P. A. Pincus, Phys. Kondens. Mater. **11**, 189 (1970).
[47]G. S. Rushbrooke, G. Stell, and J. S. Hoye, Mol. Phys. **26**, 1199 (1973).
[48]J. J. Weis and D. Levesque, Phys. Rev. Lett. **71**, 2729 (1993).
[49]R. P. Sear, Phys. Rev. Lett. **76**, 2310 (1996).
[50]R. van Roij, Phys. Rev. Lett. **76**, 3348 (1996).
[51]P. I. C. Teixeira, J. M. Tavares, and M. M. Telo da Gama, J. Phys.: Condens. Matter **12**, R411 (2000).
[52]G. Ganzenmüller and P. J. Camp, J. Chem. Phys. **126**, 191104 (2007).
[53]N. G. Almarza, E. Lomba, C. Martín, and A. Gallardo, J. Chem. Phys. **129**, 234504 (2008).
[54]F. Sciortino, A. Giacometti, and G. Pastore, Phys. Chem. Chem. Phys. **12**, 11869 (2010).
[55]A. Z. Panagiotopoulos, M. A. Floriano, and S. K. Kumar, Langmuir **18**, 2940 (2002).
[56]F. Lo Verso, A. Z. Panagiotopoulos, and C. N. Likos, Phys. Rev. E **79**, 010401 (2009).
[57]K. V. Workum and J. F. Douglas, Phys. Rev. E **71**, 031502 (2005).
[58]J. P. K. Doye, A. A. Louis, I.-C. Lin, L. R. Allen, E. G. Noya, A. W. Wilber, H. C. Kok, and R. Lyus, Phys. Chem. Chem. Phys. **9**, 2197 (2007).
[59]Q. Chen, S. Bae, and S. Granick, Nature (London) **469**, 381 (2011).
[60]F. Romano and F. Sciortino, Soft Matter **10**, 171 (2011).
[61]N. Geerts and E. Eiser, Soft Matter **6**, 4647 (2010).